

Cite this article as: Zhao Chenmeng, Wu Hao, Zhang Jifeng, et al. Effect of Nb Addition on Microstructure and Mechanical Properties of $\text{Fe}_{0.5}\text{MnNi}_{1.5}\text{CrNb}_x$ High-Entropy Alloys[J]. Rare Metal Materials and Engineering, 2021, 50(08): 2783-2788.

ARTICLE

Effect of Nb Addition on Microstructure and Mechanical Properties of $\text{Fe}_{0.5}\text{MnNi}_{1.5}\text{CrNb}_x$ High-Entropy Alloys

Zhao Chenmeng¹, Wu Hao¹, Zhang Jifeng¹, Zhu Heguo¹, Xie Zonghan²

¹College of Materials Science and Engineering, Nanjing University of Science and Technology, Nanjing 210094, China; ²School of Mechanical Engineering, University of Adelaide, SA 5005, Australia

Abstract: $\text{Fe}_{0.5}\text{MnNi}_{1.5}\text{CrNb}_x$ ($x=0, 0.05, 0.1$, molar ratio) high-entropy alloys were prepared by vacuum induction melting. The effect of Nb content on the microstructure and mechanical properties of the new alloy was analyzed. The results show that the Nb-free alloy has a single-phase fcc structure, and its tensile strength and elongation to failure (i.e., ductility) are 519 MPa and 47%, respectively. With the addition of Nb ($x=0.05$), the (200) texture and Fe_2Nb Laves phase appear. The ductility of alloy increases to 55%, while the tensile strength increases to 570 MPa. When the molar ratio of Nb increases to 0.1, the texture diminishes, whereas the volume fraction of the Fe_2Nb phase is increased. The resultant tensile strength and ductility are 650 MPa and 45%, respectively.

Key words: high-entropy alloy; Nb doping; microstructure; Laves phase; mechanical properties

High-entropy alloys have superior properties to those of traditional alloys due to their special structure. They are typically made of single fcc or bcc phase or their mixture. In some cases, a small amount of intermetallic compounds are also identified in solid solution matrix^[1-5]. While high-entropy alloys often have excellent plasticity due to their simple structures, the tensile strength remains to be improved for structural applications^[6-9]. To address this issue, Jiang et al^[10] added Ta to CoCrFeNi high-entropy alloy at a molar ratio of 0.5 and increased the yield strength of the alloy from 145 MPa to 1346 MPa. In other study, a small amount of Nd was incorporated to CoCrFeMnNi high-entropy alloy^[11], and the tensile strength of the alloy increases from 590 MPa to 820 MPa. A previous investigation also found that by increasing Al content, $\text{Al}_x\text{CoCrCuFeNi}$ high-entropy alloy changed first from fcc to fcc+bcc structure and then to single bcc phase structure. In doing so, lattice distortion deepened, leading to the strength increase^[12]. In addition, it is found that the addition of alloying elements such as Ti, V, and Pd to high entropy alloys can improve the mechanical properties of materials^[13-16]. Fu et al^[17-19] found that the unequal-atomic $\text{CoNiFeCrAl}_{0.6}\text{Ti}_{0.4}$ high-entropy alloy has nanoscale twins after spark plasma sintering. The yield stress, compressive

strength, compression ratio and Vickers hardness of the alloy are 2.08 GPa, 2.52 GPa, 11.5% and 5730 MPa, respectively. The $\text{CoNiFeCrAl}_{0.6}\text{Ti}_{0.4}$ high entropy alloy displays excellent comprehensive mechanical properties due to the effect of nanoscale twins. Unequal-atomic $\text{Al}_{0.6}\text{CoNiFeTi}_{0.4}$ high-entropy alloy prepared by mechanical alloying and spark plasma sintering has excellent mechanical properties at room temperature (yield stress ~ 2732 MPa; compressive strength ~ 3172 MPa). In other study^[20], the nanoscale twins appear in fcc phase of $\text{Al}_{0.4}\text{FeCrCo}_{1.5}\text{NiTi}_{0.3}$ high-entropy alloy, which makes the alloy have great mechanical properties. It can be seen that changing the content of one or several elements in the high-entropy alloy markedly affects the microstructure and properties of the alloy. In the previous work, it is found that $\text{Fe}_{0.5}\text{MnNi}_{1.5}\text{Cr}$ alloy has good plasticity but inferior tensile strength. It is known that alloying elements with a large difference in atomic radius from the matrix affects the microstructure and mechanical properties of the alloys^[14,21-24]. Nb has a high melting point and is often added to refractory materials to improve their high temperature strength. Its atomic radius is 0.146 nm, and the difference in atomic radius between Nb and the $\text{Fe}_{0.5}\text{MnNi}_{1.5}\text{Cr}$ alloy components such as Fe (0.126 nm), Mn (0.126 nm), Ni (0.124 nm) and Cr (0.127

Received date: August 08, 2020

Foundation item: Science and Technology Advancement Project in Jiangsu Province (BE2018753/KJ185629); National Natural Science Foundation of China (51571118, 51371098); 2020 Extracurricular Academic Research Fund for College Students of Nanjing University of Science and Technology

Corresponding author: Zhu Heguo, Ph. D., Professor, Nanjing University of Science and Technology, Nanjing 210094, P. R. China, E-mail: zhg1200@sina.com

Copyright © 2021, Northwest Institute for Nonferrous Metal Research. Published by Science Press. All rights reserved.

nm) is quite large. In addition, the relatively low density of Nb as compared to other high-melting elements can reduce the alloy mass^[25,26].

In this experiment, the effect of Nb addition on Fe_{0.5}MnNi_{1.5}CrNb_x high entropy alloys was studied, and the strengthening mechanism was analyzed to guide the design of the high-entropy alloys with high strength and enhanced plasticity.

1 Experiment

The vacuum induction heating method was used to heat the mixture of Fe, Mn, Ni, Cr, and Nb particles with a purity of 99.99% (Table 1) to a molten state. After thorough mixing, the molten metal was poured into a copper mold and cooled down to the room temperature in the furnace. The size of as-cast samples is shown in Fig. 1. During the entire process, the furnace always maintained an argon atmosphere to prevent the sample from being oxidized or contaminated.

I-shaped tensile specimens (length ~10.6 mm; width ~2.0 mm; and thickness ~1.5 mm) were prepared by wire electrical discharge machining (WEDM). The tensile testing was performed to determine the mechanical properties of the material at room temperature. The tensile fracture surface was observed by a scanning electron microscope (SEM, FEI Duanta 250F) at a voltage of 20 V. X-ray diffractometer (XRD, Bruker-AXS D8 Advance) with a Cu K α radiation, SEM, and energy dispersive spectrometer (EDS, FEI Duanta 250F) were used to characterize the crystal structure, microstructure, and element distribution of the alloys, respectively. The scanning angle of XRD ranged from 20° to 80° at a speed of 6°/min. Before the SEM analysis, the

Table 1 Chemical composition of Fe_{0.5}MnNi_{1.5}CrNb_x samples (wt%)

Sample	Fe	Mn	Ni	Cr	Nb
Nb0	12.5	25	37.5	25	0
Nb0.05	12.3	24.6	36.9	24.6	1.23
Nb0.1	12.2	24.4	36.6	24.4	2.44

Note: Fe_{0.5}MnNi_{1.5}CrNb_x ($x=0, 0.05, 0.1$, molar ratio) are named as Nb0, Nb0.05 and Nb0.1, respectively.

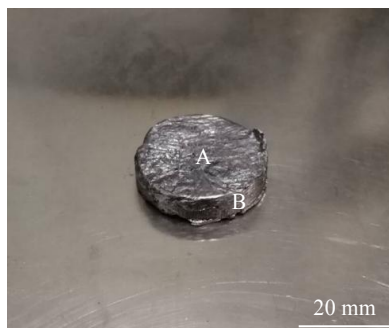


Fig.1 Optical image of as-cast sample (A represents the top surface and B denotes side surface or surface vertical to A)

samples were corroded with aqua regia for 20 s. The observation was performed along two directions, one parallel to the A surface and the other along the B surface (Fig. 1). Accordingly, the samples parallel to the A surface are named as A-Nbx and the samples parallel to the B surface are named as B-Nbx, where x represents the Nb content in molar ratio.

2 Results

2.1 Microstructure features

Fig.2 shows the XRD patterns of Nbx. Fig.2a~2c are the XRD patterns obtained from samples Nb0, Nb0.05 and Nb0.1, respectively. The different Nb contents cause the change of alloy crystal structure. The (111) diffraction peak intensities of both A-Nb0 and B-Nb0 samples are low, but the (200) plane diffraction peaks of B-Nb0 are high (Fig.2a). The intensity of the (200) plane diffraction peak of the A-Nb0.05 sample remains high, while the intensity of the fcc diffraction peak in B-Nb0.05 is low (Fig.2b). Fig.2d represents XRD patterns of A-Nbx samples. In comparison, Nb0.1 is dominated by fcc diffraction peaks (Fig. 2c), where the difference in intensity between the (111) and (200) diffraction peaks is reduced. In addition to the fcc peak, some other diffraction peaks appear near the (111) diffraction peak, which correspond to the Laves phase with Nb (Fig.2d). According to PDF card, the Nb-rich phase is Fe₂Nb. For the B-Nb0.1 sample, the intensities of the (200) peak and the Laves phase diffraction peak around the (111) are quite low. In addition, Fig. 2e shows the partially enlarged view of diffraction angle from 45° to 55° in Fig.2d. The diffraction peak shifts slightly to the left and then to the right as the Nb content increases.

Fig.3a~3c show the SEM images of A-Nb0, A-Nb0.05, and A-Nb0.1 samples, respectively. The grain boundaries of the A-Nb0 sample are evident, revealing equiaxed grains. Uniformly distributed corrosion pits (artifacts from sample preparation) can be seen but no precipitates are discernible on the surface. In comparison, the grain boundaries in A-Nb0.05 and A-Nb0.1 samples are not visible and the alloys show a dendritic structure. The corrosion pits are evenly distributed, and worm-like white precipitates appear within them. It is worth noting that the volume fraction of the corrosion pits in A-Nb0.1 is larger, and there are precipitates in each pit. In the sample A-Nb0.05, however, the precipitates only appear in some corrosion pits. Fig.3d and 3e illustrate the SEM images of B-Nb0.05 and B-Nb0.1 samples, respectively. The B-Nb0.05 sample has a dendritic structure, the equiaxed corrosion pits are parallel to the dendrites, and some corrosion pits contain worm-like precipitates. Fig.3f is a high magnification SEM image of B-Nb0.05 sample. The yellow dotted line is used to highlight the grain boundaries, which shows that the corrosion pits are distributed along the grain boundaries. The B-Nb0.1 sample also shows a dendritic structure (Fig.3e).

Fig. 4 shows the high magnification SEM image of A-Nb0.1. White worm-like particles appear in most of the corrosion pits between the dendrites, and the corrosion pits are randomly distributed. The EDS analysis results of the

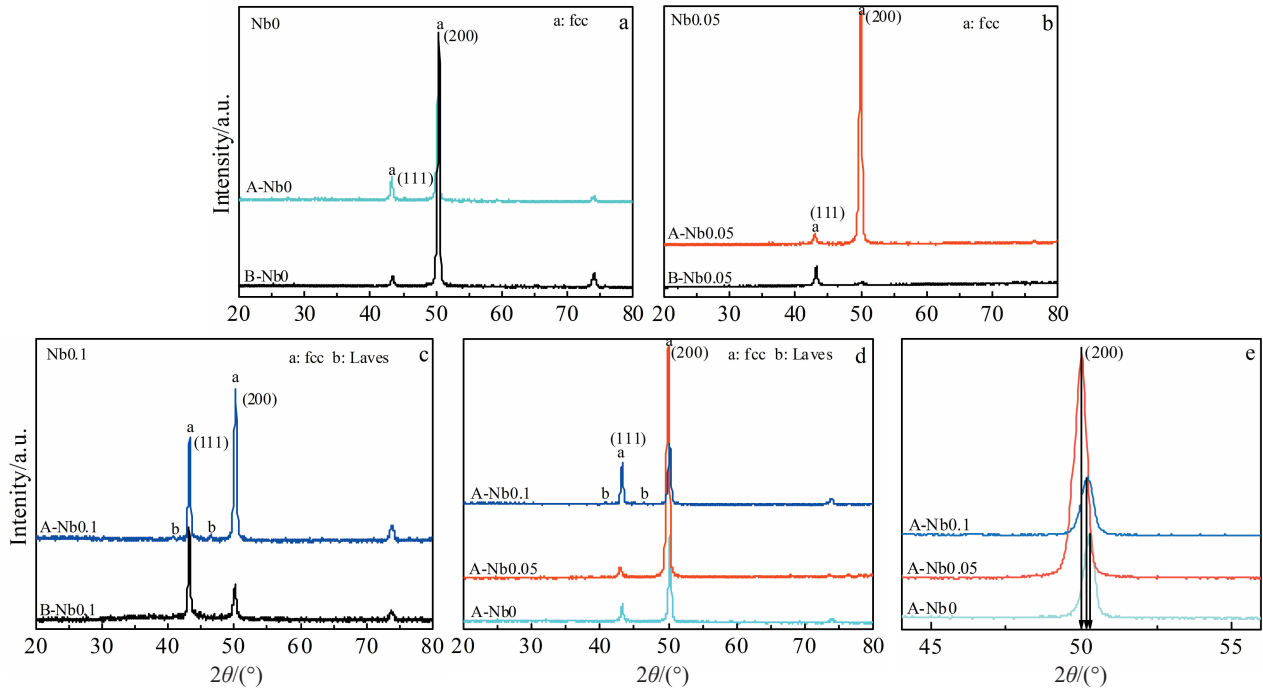


Fig.2 XRD patterns of Nb0 (a), Nb0.05 (b), Nb0.1 (c), and A-Nbx (d, e) samples

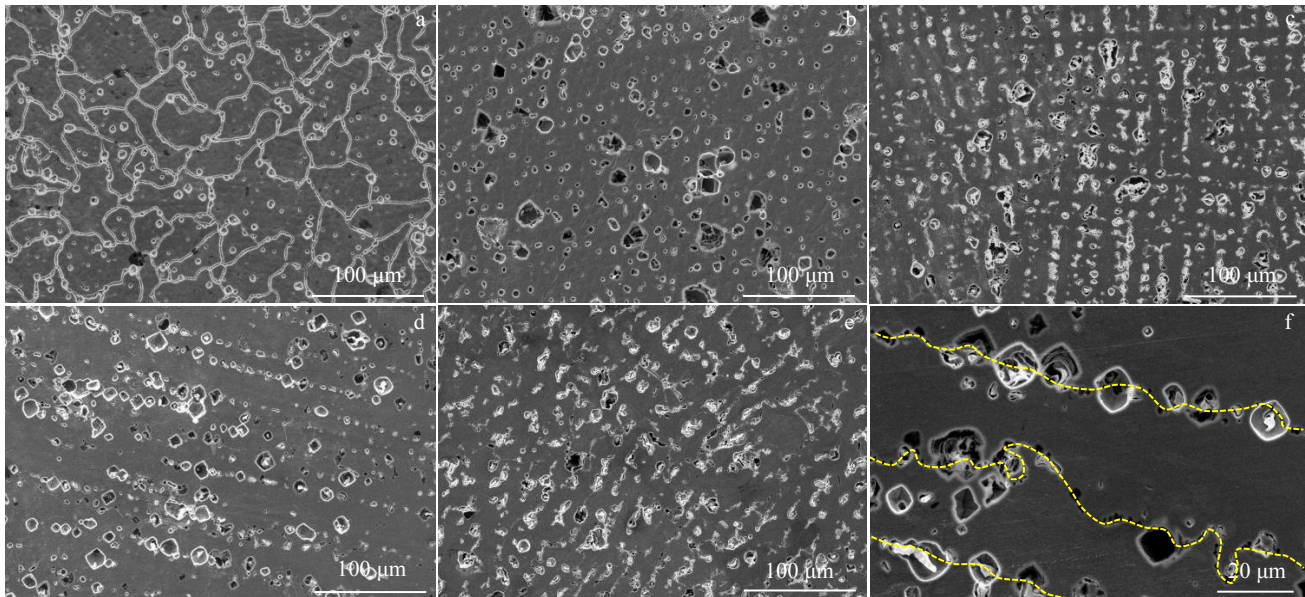


Fig.3 SEM images of A-Nb0 (a), A-Nb0.05 (b), A-Nb0.1 (c), B-Nb0.05 (d, f) and B-Nb0.1 (e) samples

precipitates (region A) and the matrix (region B) are shown in Table 2. It can be seen that the precipitates are Laves phase with Nb (region A), which is consistent with the XRD results (Fig. 2c). However, the Laves phase diffraction peak is not detected in the sample Nb0.05, which might be due to the fact that the volume fraction of Laves phase in the sample Nb0.05 is too low to be identified by XRD. While the chemical composition of as-cast Nb0.1 alloy matrix is close to the nominal value.

Fig.5 illustrates the tensile fracture surfaces of the samples Nb0, Nb0.05, and Nb0.1. Table 3 shows the atomic percentage of elements in sediments. All the fractures exhibit equiaxed dimples which are uniformly distributed. Meanwhile, sediments appear within some dimples, which are Mn-rich precipitates according to the EDS analysis (Table 3). For the sample Nb0, the dimples are deep and large in size; the dimples in the sample Nb0.05 are shallower but similar in

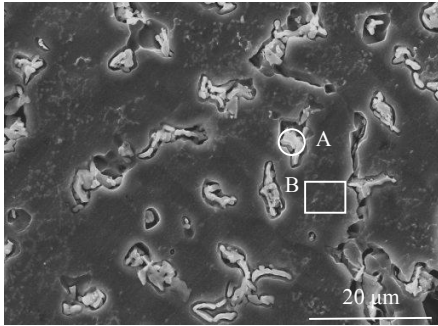


Fig.4 High magnification SEM image of sample A-Nb0.1

Table 2 EDS analysis results of different regions of sample Nb0.1 marked in Fig.4 (at%)

Region	Fe	Mn	Ni	Cr	Nb
A	9.61	24.83	34.08	20.40	11.09
B	13.04	24.10	35.26	26.31	1.30
Nominal	12.20	24.40	36.60	24.40	2.44

size, and the number of the Mn-rich precipitates in the dimples increases significantly. When the Nb content increases to $x=0.1$, the size of the dimples becomes smaller, and the dimples still contain Mn-rich precipitates, but their number is greatly reduced. All three alloys show typical ductile fracture.

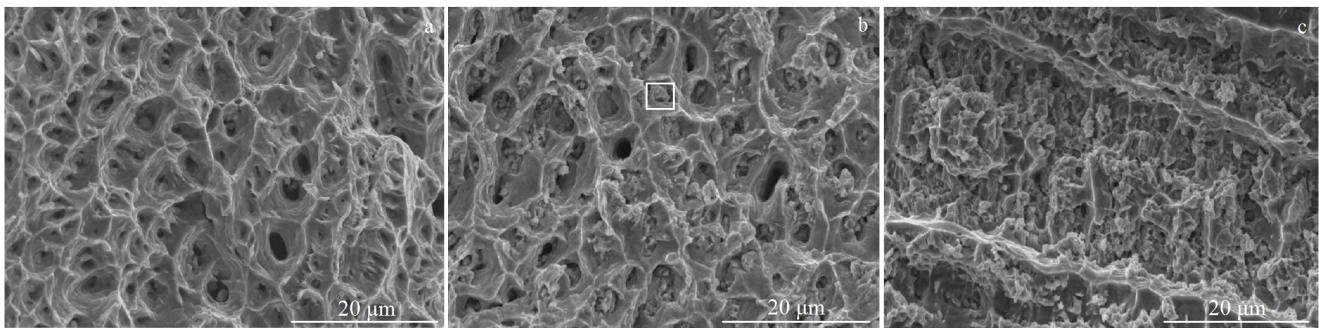


Fig.5 Fracture surface morphologies of samples Nb0 (a), Nb0.05 (b), Nb0.1 (c)

Table 3 EDS analysis results of sediments (at%)

Fe	Mn	Ni	Cr	Nb
23.90	54.16	7.79	13.99	0.16

2.2 Mechanical properties

Fig. 6 is the tensile engineering stress-strain curve of the Nb x samples. It can be seen that the elongation of all the three samples exceeds 40%. Among them, the elongation of Nb0 samples is up to 47%, but the tensile strength is relatively low (519 MPa). When the molar ratio of Nb is 0.05, both the ductility and tensile strength of the alloy are improved (i.e., the tensile strength is increased to 570 MPa, and the elongation is also 55%). As the Nb content further increases to 0.1, the tensile strength is increased to 650 MPa but the ductility is reduced to 45%.

3 Discussion

3.1 Phase stability

The phase stability of high-entropy alloys is affected by many factors, including mixed entropy (ΔS_{mix}), mixed enthalpy (ΔH_{mix}), mismatch (δ), interaction parameter (Ω), etc. When the atomic mismatch $\delta < 6.6\%$ and interaction parameter $\Omega > 1.1$, a simple solid solution phase tends to form^[27]. It is easier to form a stable solid solution when the size of different atoms is similar. There is severe lattice distortion and high strain energy in the formed solid solution when $\delta > 6.6\%$. δ can be

calculated by the following formula^[20,28,29]:

$$\delta = \sqrt{\sum_{i=1}^n c_i \left(1 - \frac{r_i}{r}\right)^2} \quad (1)$$

$$r = \sum_{i=1}^n r_i c_i \quad (2)$$

where r and r_i are the average atomic radius and the atomic radius of each component, respectively; c_i is the atomic ratio of each component (already listed in Table 1). The formula for calculating the interaction parameters is as follows^[28,30]:

$$\Omega = \frac{T_m \Delta S_{\text{mix}}}{|\Delta H_{\text{mix}}|} \quad (3)$$

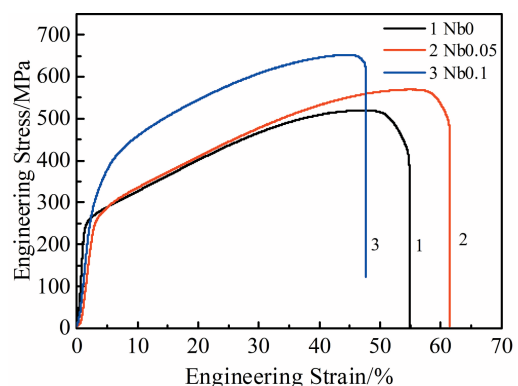


Fig.6 Tensile engineering stress-strain curves of three Nb x alloys

$$\Delta S_{\text{mix}} = -R \sum_{i=1}^n (c_i \ln c_i) \quad (4)$$

$$T_m = \sum_{i=1}^n c_i (T_m)_i \quad (5)$$

$$\Delta H_{\text{mix}} = 4 \sum_{i \neq j}^n \Delta H_{ij}^{\text{mix}} c_i c_j \quad (6)$$

where R is the ideal gas constant ($R=8.314 \text{ J}\cdot\text{mol}^{-1}\cdot\text{K}^{-1}$), and T_m is the melting point (K). The calculation results are shown in Table 4. It can be seen that δ of alloys with different Nb contents does not exceed 6.6%, and the Ω is greater than 1.1, so a solid solution structure can be obtained. However, according to XRD and SEM results, there are Laves phase in alloys when $x \geq 0.05$. It indicates that there is other more important factor affecting the structure of the alloy. The prerequisite for using Ω to determine the phase structure is that the atomic sizes are similar^[27-28]. According to Fig.2e, as the Nb content increases, the (200) peak shifts slightly to the left and then to the right. This phenomenon indicates that lattice distortion first increases and then decreases. Due to the difference in radius between Nb and other atoms, lattice distortion increases with adding Nb, while the precipitation of the Nb-rich phase leads to the decrease of lattice distortion. While the decrease of lattice distortion leads to the reduction of strain energy of the alloy.

3.2 Microstructure development

With the increase of Nb content, the fcc (200) diffraction peak first shifts to the left (Fig.2e) and then to the right. This is due to the increase in the degree of lattice distortion after the Nb with a larger atomic radius occupies the lattice position in the solid solution. By further increasing the Nb content, however, the lattice distortion promotes the precipitation of the second phase, which reduces the Nb atoms in the matrix, and lowers the level of lattice distortion in the matrix.

According to Fig.3 and Fig.4, Nb-rich Laves phase appears in both Nb0.05 and Nb0.1 samples, in which the Fe and Cr contents are relatively small (Table 2) but the Ni contents are large. The enthalpy of mixing is an important parameter to predict the formation of phase conformation. The mixing enthalpies of Nb-Fe, Nb-Mn, Nb-Ni, and Nb-Cr are -16, -4, -30, and -7 kJ/mol, respectively^[31]. A high Ni content in the Nb-rich precipitates is attributed to the lowest mixing enthalpy of Ni-Nb among the four elements.

3.3 Mechanical properties

Compared with those of the Nb0 sample, the tensile strength (increasing from 519 MPa to 570 MPa) and the ductility (47% to 55%) of sample Nb0.05 increase simultaneously (Fig.6). The reasons for the increase in strength are given as follows. First, the addition of Nb with a larger atomic radius causes lattice distortion, which increases the resistance to

dislocation slip. Second, the formation of a small amount of Nb-rich precipitates pins the movable dislocations so that the dislocation slip requires higher stress. In addition, the grain shape, distribution and size also affect the mechanical properties of the alloy^[5,32-34]. When the Nb content is increased to $x=0.1$, the grain shape changes from equiaxed to short dendrites (Fig.3). As the grains are refined and the interfacial area is increased, the tensile strength is further increased (650 MPa). In addition, the mechanical properties, volume fraction, size and distribution of the second phase in the matrix are important factors affecting the mechanical properties of the material^[10,31,35-38]. Fig.3 shows that when the content of Nb is increased, the volume fraction of the precipitates in the Nb0.1 sample increases. As such, the dispersion strengthening effect of the Nb-rich Laves phase is enhanced. The elongation of the sample Nb0.1 decreases to 45%. The possible reason is that the distribution of the Nb-rich Laves phase in the matrix interrupts the continuity of the matrix, and stress concentration occurs near the interface between the two phases during the tensile tests, causing fracture.

4 Conclusions

1) The $\text{Fe}_{0.5}\text{MnNi}_{1.5}\text{Cr}$ alloy has a single-phase fcc structure. With the increase of Nb content, Nb-rich Laves phase appears and increases in volume fraction.

2) The tensile strength of $\text{Fe}_{0.5}\text{MnNi}_{1.5}\text{CrNb}_x$ alloys increases from 519 MPa to 650 MPa, while the ductility first increases to 55% and then decreases to 45%. Both precipitation strengthening and solid solution strengthening are responsible for enhanced strength.

3) When the Nb content is $x=0.1$, both tensile strength (650 MPa) and ductility (45%) of the $\text{Fe}_{0.5}\text{MnNi}_{1.5}\text{CrNb}_{0.1}$ alloy are high, and as such, the alloy has potential for load-bearing applications.

References

- 1 Sang L M, Xu Y. *Journal of Non-Crystalline Solids*[J], 2020, 530: 119 854
- 2 Kong D, Guo J, Liu R W et al. *Intermetallics*[J], 2019, 114: 106 560
- 3 Xie Y H, Zhou D S, Luo Y F et al. *Materials Characterization* [J], 2019, 148: 307
- 4 Ding Q Q, Zhang Y, Chen X et al. *Nature*[J], 2019, 574 (7777): 224
- 5 Sathiaraj G D, Pukenas A, Skrotzki W. *Journal of Alloys and Compounds*[J], 2020, 826: 154 183
- 6 Klimova M V, Semenyuk A O, Shaysultanov D G et al. *Journal of Alloys and Compounds*[J], 2019, 811: 152 000
- 7 Otto F, Dlouhy A, Somsen C et al. *Acta Mater*[J], 2013, 61(15): 5743
- 8 Schuh B, Mendez-Martin F, Volker B et al. *Acta Mater*[J], 2015, 96: 258
- 9 He J Y, Zhu C, Zhou D Q et al. *Intermetallics*[J], 2014, 55: 9

Table 4 r , ΔS_{mix} , T_m , ΔH_{mix} , δ and Ω value of Nb $_x$ samples

Sample	r/nm	$\Delta S_{\text{mix}}/\text{J}\cdot\text{K}^{-1}\cdot\text{mol}^{-1}$	T_m/K	$\Delta H_{\text{mix}}/\text{kJ}\cdot\text{mol}^{-1}$	$\delta/\%$	Ω
Nb0	0.1255	10.977	1785.3	-3.6250	0.08	5.41
Nb0.05	0.1253	11.465	1790.4	-6.2210	0.021	3.30
Nb0.1	0.1260	11.663	1809.3	-6.7752	0.027	3.11

- 10 Jiang H, Han K M, Qiao D G et al. *Materials Chemistry and Physics*[J], 2018, 210: 43
- 11 Wang C, Li T H, Liao Y C et al. *Materials Science and Engineering A*[J], 2019, 764: 138 192
- 12 Tong C J, Chen Y L, Chen S K. *Metallurgical and Materials Transactions A*[J], 2005, 36A(5): 1263
- 13 Lucas M S, Mauger L, Munoz J A et al. *Journal of Applied Physics*[J], 2011, 109(7): 307
- 14 Liu W H, Wu Y, He J Y et al. *Journal of the Minerals, Metals and Materials Society*[J], 2014, 66: 1973
- 15 Wu H, Huang S R, Zhu C Y et al. *Materials Letters*[J], 2019, 257: 126 729
- 16 Zhang M D, Zhang L J, Fan J T et al. *Materials Science and Engineering A*[J], 2019, 764: 138 212
- 17 Fu Z Q, Chen W Q, Fang S C et al. *Journal of Alloys and Compounds*[J], 2013, 553: 316
- 18 Chen W P, Fu Z Q, Fang S C et al. *Materials Science and Engineering A*[J], 2013, 565: 439
- 19 Fang S C, Chen W P, Fu Z Q. *Materials and Design*[J], 2014, 54: 973
- 20 Yang S F, Zhang Y, Yan X et al. *Materials Chemistry and Physics* [J], 2018, 210: 240
- 21 Chen M R, Lin S J, Yeh J W et al. *Materials Transactions*[J], 2006, 47(5): 1395
- 22 Liu W H, Wu Y, He J Y et al. *Scripta Materialia*[J], 2013, 68(7): 526
- 23 Tang Z, Diao H Y, Yang T F et al. *Journal of the Minerals, Metals and Materials Society*[J], 2013, 65: 1848
- 24 Tian F Y, Delczeg L, Chen N X et al. *Physical Review B*[J], 2013, 88(8): 85 128
- 25 Yu Y, He F, Qiao Z H et al. *Journal of Alloys and Compounds*[J], 2019, 775: 1376
- 26 Zhang Y, Liu Y, Li Y X et al. *Materials Letters*[J], 2016, 174: 82
- 27 Yang X, Zhang Y. *Materials Chemistry and Physics*[J], 2012, 132: 233
- 28 Liu W H, He J Y, Huang H L et al. *Intermetallics*[J], 2015, 60: 1
- 29 Liu Y, Zhang Y, Zhang H et al. *Journal of Alloys and Compounds* [J], 2017, 694: 869
- 30 Zhang Y, Zhou Y J, Lin J P et al. *Advanced Engineering Materials*[J], 2008, 10: 534
- 31 Takeuchi A, Inoue A. *Materials Transactions*[J], 2005, 46(12): 2817
- 32 Fu A. *Journal of Alloys and Compounds*[J], 2020, 815: 152 466
- 33 Luo W Y. *Journal of Alloys and Compounds*[J], 2018, 754: 163
- 34 Fan Q C, Li B S, Zhang Y. *Materials Science and Engineering A* [J], 2014, 598: 244
- 35 Abdulkadir Amar, Li J F. *Intermetallics*[J], 2019, 109: 162
- 36 Abbasi E, Dehghani K. *Materials Science and Engineering A*[J], 2019, 753: 224
- 37 Xie Y H, Zhou D H, Luo Y F et al. *Materials Characterization* [J], 2019, 148: 307
- 38 Nawrockia J, Motyka M, Szeliga D et al. *Journal of Manufacturing Processes*[J], 2020, 49: 153

Nb 含量对 Fe_{0.5}MnNi_{1.5}CrNb_x 高熵合金微观结构和力学性能的影响

赵晨朦¹, 伍 昊¹, 张继峰¹, 朱和国¹, 谢宗翰²

(1. 南京理工大学材料科学与工程学院, 江苏 南京 210094)

(2. 阿德莱德大学机械工程学院, 澳大利亚 阿德莱德 5005)

摘要: 采用真空感应熔炼法制备了 Fe_{0.5}MnNi_{1.5}CrNb_x ($x=0, 0.05, 0.1$, 摩尔比) 高熵合金, 并分析了不同 Nb 含量对其组织和力学性能的影响。结果表明, 不含 Nb 元素的合金具有单相 fcc 结构, 其抗拉强度和断裂延伸率 (即延展性) 分别为 519 MPa 和 47%。添加少量的 Nb ($x=0.05$) 后出现 (200) 织构和少量 Fe₂Nb Laves 相, 合金的延展性增加到 55%, 并且抗拉强度增加到 570 MPa。当 Nb 含量增加到 $x=0.1$ 时, 织构减少, 而 Fe₂Nb Laves 相增多, 抗拉强度和延展性分别为 650 MPa 和 45%。

关键词: 高熵合金; Nb 掺杂; Laves 相; 微观组织; 力学性能

作者简介: 赵晨朦, 女, 1997年生, 硕士生, 南京理工大学材料科学与工程学院, 江苏 南京 210094, E-mail: 18251969169@163.com